



Orbital Debris Quarterly News

Volume 21, Issue 3
August 2017

Inside...

Update on the
Space Debris
Sensor2

ODPO Adopts
a Logo2

Benefits of a
High LEO *In-Situ*
Measurement
Mission3

DAS Reentry Risk
Analysis: Mission
Planning for
Compliance with
NASA Standards6

Conference
Reports9

Space Missions
and Satellite
Box Score12



A publication of
the NASA Orbital
Debris Program Office

Earliest Delta Rocket Body Fragmentation Determined

Air Force Space Command analysts have recently disclosed the discovery of the earliest Delta second stage rocket body to have fragmented on-orbit. The Delta model N rocket body (International Designator 1968-114B, U.S. Strategic Command [USSTRATCOM] Space Surveillance Network [SSN] catalog number 3616) launched the ESSA 8 (TOS-F) spacecraft. The rocket body is assessed to have fragmented on 15 November 1973 after having been on-orbit 4.9 years and was in a 1462 x 1413 km altitude, 101.6° inclination orbit at the time of the event. Potential stored energy sources include batteries, a cold gas attitude control system, propellant pressurization gas, and residual hypergolic propellants. In addition to the parent body, 17 additional fragments (piece tags E-W, SSN 42078-42094 inclusive) have entered the public satellite catalog as of 4 June 2017. The fragments are plotted on a standard Gabbard diagram in the figure.

This event supersedes the fragmentation of the NOAA 3 Delta second-stage rocket body (International Designator 1973-086B, USSTRATCOM SSN 6921) as being the first Delta to fragment—by approximately 43 days.

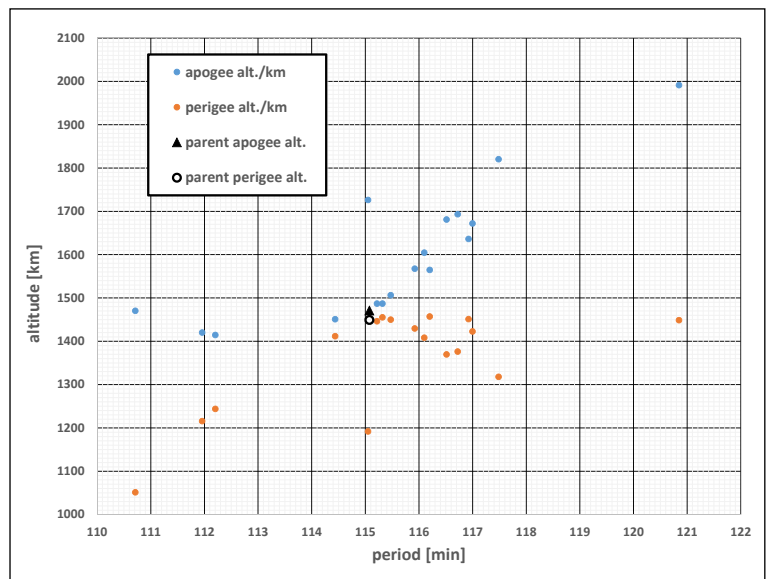
This launch, also known as “Delta 62,” occurred well before the introduction of now-standard mitigation practices inaugurated, on an informal basis, by Delta 155

in August 1981. However, an assessment of Delta rocket bodies remaining on-orbit prior to the introduction of informal or formal passivation practices (ODQN, vol. 6, issue 3, July 2001, pp. 7-8, “A Fragmentation Assessment of Legacy Delta Rocket Bodies”) had noted that the five Delta model N second stages had exhibited no signs of fragmentation events at the time of writing. From that article, revised slightly for clarification:

“Several changes differentiate an N model second stage from the 100 (and later) series.

Physically, the model N and 100 series were stressed for aerodynamic flight, while the 1000 series introduced the so-called “straight 8” configuration,

continued on page 3



A Gabbard diagram illustrates the event’s energetic nature. Fragments now span over 10 minutes in period and 940 km in altitude.

Update on the Space Debris Sensor

The Space Debris Sensor (SDS) is scheduled to launch in the trunk of the SpaceX 13 Dragon spacecraft capsule in November 2017. After the capsule is mated to the International Space Station (ISS), the robotic arm will remove the sensor from the trunk and attach it to the Columbus Module external payload facility. The SDS will be mounted facing the velocity vector and will remain there for at least 3 years collecting data on the small debris environment at the ISS.

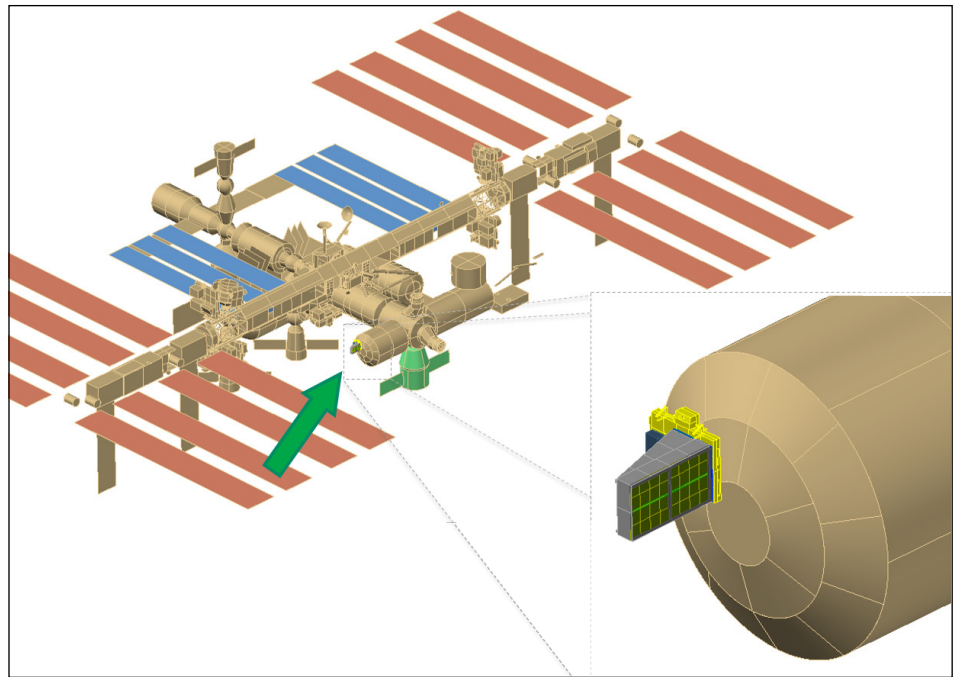
The SDS is a technology demonstration designed to determine how well a combination of detection methods can be used to characterize the size, speed, direction, and density of debris smaller than 1 mm that hits the sensor (ODQN, vol. 21, issue 1, February 2017, p.1, “*Space Debris Sensor Waiting for Launch*” and ODQN, vol. 19, issue 1, January 2015, pp. 2 – 3, “*DRAGONS to Fly on the ISS*”).

After the mission is complete, the SDS will be placed in a Dragon trunk for disposal during re-entry. The knowledge from this mission will be used to update orbital debris models and help in the development of future sensors that will be placed in higher orbits where the small debris environment has never been directly measured.

More information about the utility and potential role of SDS-derived sensors in

monitoring the debris population at altitudes higher than that of ISS/SDS is in the article

“*Benefits of a High LEO In-Situ Measurement Mission*” in this issue of the ODQN. ♦

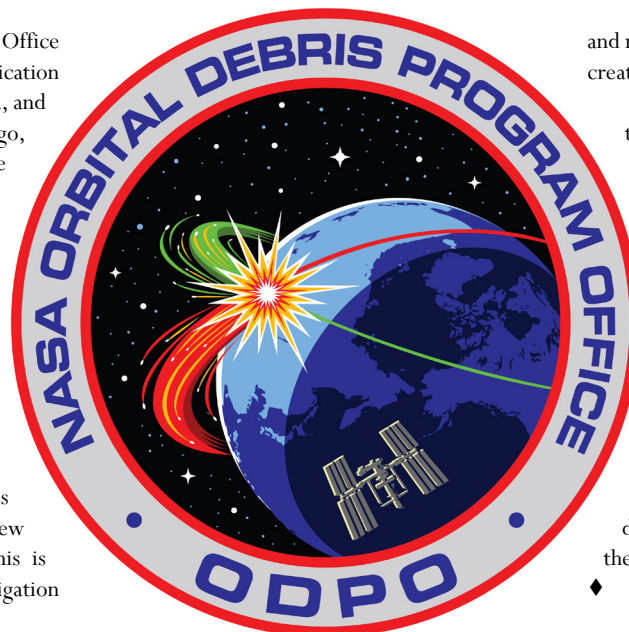


The SDS will be hosted aboard ISS on the Columbus module External Payload Facility (EPF)-Starboard Overhead X-location (SOX), as indicated in the Figure. This location was previously used by the European Technology Exposure Facility (EuTEF); among the EuTEF payloads were two Debris In Orbit Evaluator standard MMOD measurement sensors exposed for approximately 1.57 years (15 February 2008 - 1 September 2009), which may enable a future, decadal comparison.

The Orbital Debris Program Office Adopts a Logo

The NASA Orbital Debris Program Office (ODPO) recently adopted a logo for identification at international conferences, in print media, and for public outreach. In designing the logo, we considered it important to illustrate ODPO's role as the international lead in conducting measurements and in advancing research on orbital debris to protect users of the orbital environment.

By including a figurative interpretation of a rocket body and satellite collision in low Earth orbit, our logo portrays the importance ODPO assigns to controlling the growth of the orbital debris population. In the background, representative debris and stars surround the Earth as it rotates, with a new day beginning and a bright horizon. This is meant to evoke the promise of debris mitigation



and remediation to prevent such collisions and the creation of new debris.

The International Space Station orbits the Earth, symbolizing ODPO's efforts to develop and upgrade orbital debris models to describe and characterize the current and future debris environment, thus reducing risk to operating spacecraft.

Both the design colors and the typeface were chosen to be dynamic and reproduce well in different mediums. The typeface, Eurostile LT Bold Extended, has a bold, strong presence intended to underscore ODPO's worldwide position in addressing orbital debris issues. We introduce our logo as a digital ambassador representing ODPO and the orbital debris policies that ODPO supports. ♦

Delta 62

continued from page 1

i.e., a constant eight (8) foot diameter" interstage structure that suspended the second stage inside the structure. "The most obvious visual distinction is the series 1000's annular truss encircling the second stage. Less obvious was a change in motor from the N model's Aerojet AJ10-118 (Vanguard rocket body heritage) to the 100 series' AJ10-118F (Titan Transtage heritage). An examination

of all AJ10-118 powered Delta second stages to attain orbit indicates there are no fragmentation or anomalous events associated with any rocket body. Therefore, unvented N model second stages appear to present no fragmentation threat."

With the long-delayed recognition of analyst element sets being associated with Delta 62, this

conclusion is refuted. The fragmentation status of the remaining four derelict rocket bodies—those having launched ESSA 7 and 9, ITOS 1/OSCAR 5, and NOAA 1--for evidence of fragmentation in the higher-altitude sun-synchronous orbit is warranted. ♦

PROJECT REVIEW

Benefits of a High LEO *In-situ* Measurement Mission

M. MATNEY

One of the greatest challenges to understanding the most important risks to spacecraft from debris collisions is understanding the nature of debris in the millimeter size range. These debris are too small to be detected with state-of-the-art, ground-based radar or optical sensors, so we must rely on in-orbit detectors that can sample the environment at close range. The NASA Orbital Debris Engineering Model (ORDEM) 3.0 small particle environment (10 μm to approximately 1 mm) was predicated in part upon a comprehensive dataset based on post-flight inspections of the Space Shuttle windows and radiators. Because it was possible to inspect the impacts on these surfaces with electron microscopes and to identify the impactor material, we were better able to understand the differences in material of the impactors. Most significantly, a sizeable component of high-density particles was identified. These high-density particles typically cause more damage for a given size particle than lower-density particles such as aluminum. Even representing only a fraction of the total population, they can have a disproportionate effect on spacecraft risk.

Because the debris population is dynamic, especially for the small particle population where drag acts over shorter time scales, it is important to actively monitor the population. With the retirement of the Space Shuttle program in 2011, NASA no longer has a dedicated, calibrated sensor to observe the environment. In addition, *in situ* measurements, by nature, can only sample

the flux of particles at the altitudes where they fly. Models indicate that the flux of particles at Shuttle altitudes (below 600 km) may be only the proverbial "tip of the iceberg," and there may be significantly higher flux at higher altitudes between 700 and 1000 km altitude where many NASA robotic spacecraft operate.

The NASA Orbital Debris Program Office (ODPO) has been developing the technology for *in-situ* measurements of the OD environment for over a decade, and one initiative is the Debris Resistive/Acoustic Grid NASA-Navy Sensor (DRAGONS). DRAGONS uses multiple layers of thin film sensor, upon which a printed circuit of fine wires is resident. Acoustic waves in the thin film indicate time and location while the number of wires severed is proportional to orbital debris (OD) penetrator size in one dimension; multiple layers allow for a velocity and trajectory to be estimated. Two layers and a backstop also inform at least qualitative estimates of OD mass density. The DRAGONS technology has been embodied in the ODPO Space Debris Sensor, currently awaiting launch to the International Space Station. For more details, see ODQN, vol. 21, issue 1, February 2017, p.1, "*Space Debris Sensor Waiting for Launch*" and ODQN, vol. 19, issue 1, January 2015, pp. 2 – 3, "*DRAGONS to Fly on the ISS.*"

This article looks at the ORDEM 3.0 model predictions for a typical DRAGONS instrument design: a 1 m² detector facing the ram direction, and operating at a typical NASA scientific satellite orbit (altitude 705 km, inclination 98.2°) for a nominal 3-year mission. The purpose is to

determine how capable the instrument is in characterizing the environment, and how long it must operate to provide statistically significant results sufficient to update or validate our environment models. The nominal case is for a resistive grid with 75- μm -wide wires separated by 75- μm gaps.

As counting the number of severed wires is the primary way of determining particle size, a statistical model is created to estimate the number of wires a debris particle of a given size would sever. As can be seen in Fig. 1, for a given perforation-hole size, there are two possible integer numbers of wires that can be severed with varying probability.

This means that the ability of the instrument to resolve particle size (unambiguously) degrades as particles get smaller and fewer wires are severed. This "graininess" issue demonstrates the instrument has a practical lower limit for size-dependent flux estimation.

The next step is to model the flux of different debris particles at various sizes and to predict the number of times n wires are severed. The time-integrated probability of a particle size x hitting the detector is $D(x) dx$. If we assume that a particle creates a hole 1.2 times that of the particle diameter, then the probability of seeing n wires severed is $p(n | 1.2 * x)$.

The expectation value of severing n wires will be

$$\lambda_n = \int_0^{\infty} D(x) p(n | 1.2 * x) dx \quad (1)$$

continued on page 4

Benefits of a High LEO

continued from page 3

Fig. 2 shows the result of these expectation value calculations using ORDEM 3.0. We assume the DRAGONS instrument is operating well enough to resolve the difference between high-density (HD), *e.g.*, steel, and medium-density (MD), *e.g.*, aluminum, particles.

Because the actual number of severers will be a Poisson sample from these expectation values, it is necessary to fit the data to estimate the size-dependent flux. This is accomplished using a maximum likelihood method similar to that used to create the ORDEM 3.0 populations. The Monte Carlo number of severers of n wires y_n is a Poisson sample from the expectation value λ_n . The likelihood is

$$\mathcal{L} = \sum_{n=1}^{\infty} -\lambda_n + y_n \ln \lambda_n \quad (2)$$

For each Monte Carlo sample, integer values of y_n are selected (using a random Poisson sampler) from the expectation values of λ_n , using the model prediction of $D(x) dx$ derived through equation (1). Next a parameterized version of the size distribution function $D'(x) dx$ is used to compute the values of λ'_n using equation (1), and $D'(x) dx$ is varied to maximize the likelihood in equation (2). Each Monte Carlo sample will give a different fit for $D'(x) dx$. The spread of these distributions gives an estimate of the uncertainties in the size distribution estimate due to the finite sampling of impacts.

The choice of the parameterization of

the size distribution fitting is determined by how “smooth” the distribution is expected to be. Experiments for this study found that a 7-parameter log-log Fourier fit gave a good balance between smoothness and flexibility.

Fig. 3 shows the results of this process for the MD population. It seems that 75 μm is the minimum size the instrument can measure, as shown by how the uncertainty bounds diverge. The “pinches” at 75 μm and 200 μm indicate that the instrument gives very good estimates of the flux at these sizes. Above 200 μm , the uncertainties grow, until at 1 mm the uncertainties reach nearly an order of magnitude. Note that the uncertainties shrink again at about 3 mm, where the flux is fixed in the parameterization to match radar measurements. Fig. 4 shows the same chart for the HD population. Because of the lower flux of HD in the 100 μm size regime predicted by the ORDEM 3.0 model, the uncertainties here are larger, but the

instrument would still give a good estimate of the 200 μm flux.

One variant of the sensor being considered is using finer wires with smaller spacing. For comparison, Fig. 5 shows the same study as Fig. 4, but with 50 μm wires separated by 50 μm . The finer resolution is reflected in two ways. The smallest reliably measured size is now closer to 50 μm , as expected. However, the finer wires and spacing have the unexpected benefit of increasing the resolution at 1 mm, despite using the same

continued on page 5

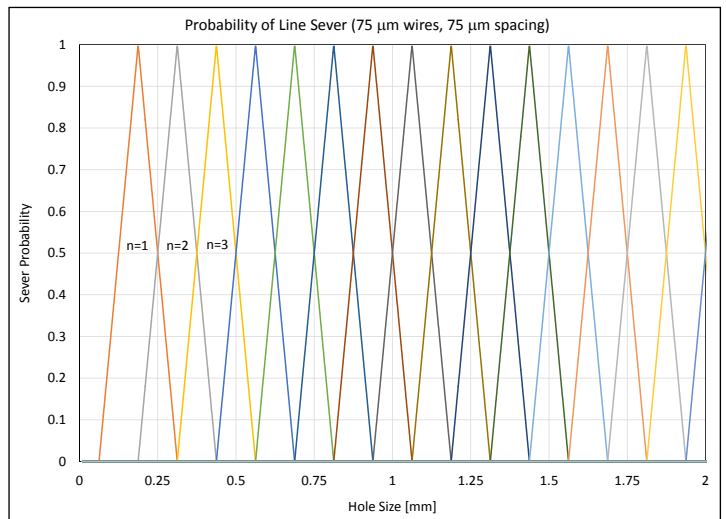


Figure 1. For a given hole size, there are, at most, two integer values (n) of the number of wires that can be severed. This is for the case of 75 μm wires separated by a 75 μm gap.

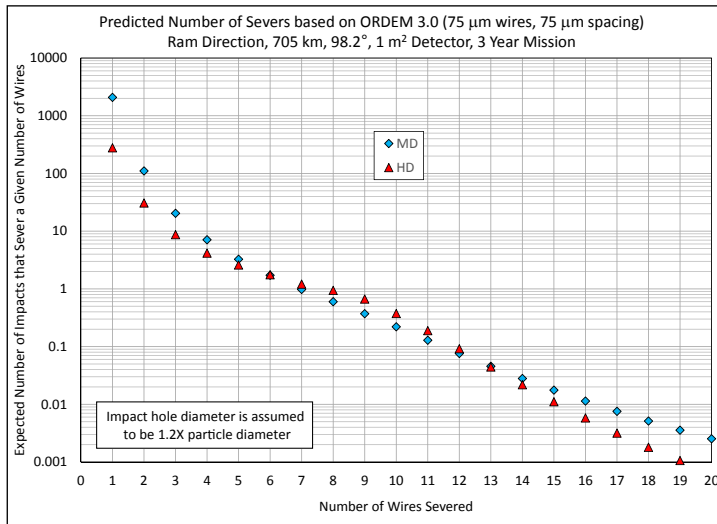


Figure 2. The predicted expectation value λ_n of the number of severers for various integer numbers of wires using the ORDEM 3.0 flux environment for the nominal mission. For this study, assume the DRAGONS instrument works as designed and can distinguish between (HD and MD debris.

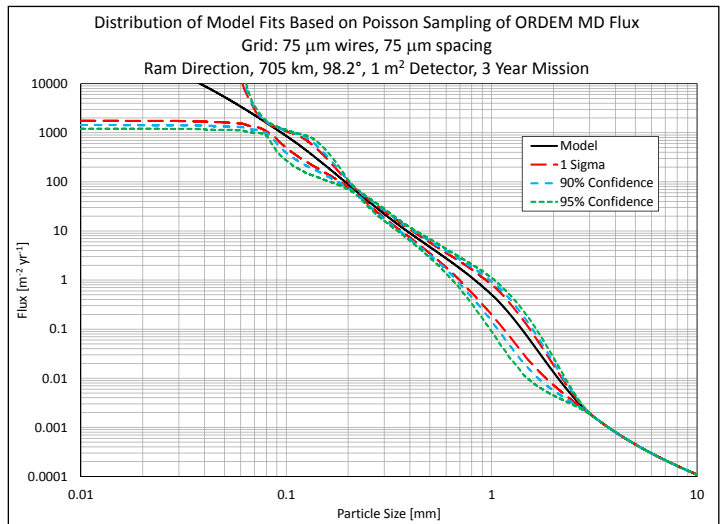


Figure 3. Using the ORDEM 3.0 model to predict the MD flux, it is possible to simulate the number of lines severed using a Monte Carlo approach. For each sample, a fit to the flux is computed. The spread in these computed size distributions shows how well the experiment can estimate the size-dependent flux. The different curves show the 1 sigma, 90%, and 95% confidence limits.

Benefits of a High LEO

continued from page 4

flux. This is due to the ability to measure the particle size to higher precision.

These results are based on the assumption that the ORDEM 3.0 model fluxes are correct, and the results show the ability to validate the model predictions. However, it is possible that the actual flux may be different from the ORDEM flux. A corollary question is whether the instrument can resolve a discrepancy between the model and actual flux. For the purpose of studying this question, a series of modified ORDEM 3.0 HD fluxes are constructed and displayed in Fig. 6; the

series reduce the 1 mm flux by various factors.

Figures 7-9 show how these modified lower fluxes are resolved by the instrument. For the 1 m² sensor in the environment for 3 years, the instrument would begin to resolve fluxes half that of the ORDEM 3.0 model.

This article demonstrates how a mission of a 1 m² detector facing the ram direction, and operating in a circular orbit at 705 km altitude and inclination 98.2° for a mission length of 3 years should be useful in validating the ORDEM model at these altitudes. The instrument should

be able to resolve a discrepancy of a factor of two between the actual flux and the predicted ORDEM model flux.

This method can also be used to study mission variations to improve the capability of resolving the environmental flux. Using a finer wire thickness and spacing reduces the uncertainties across the size spectrum. Increasing the length of time and/or surface area of the mission will also result in better resolution in

continued on page 6

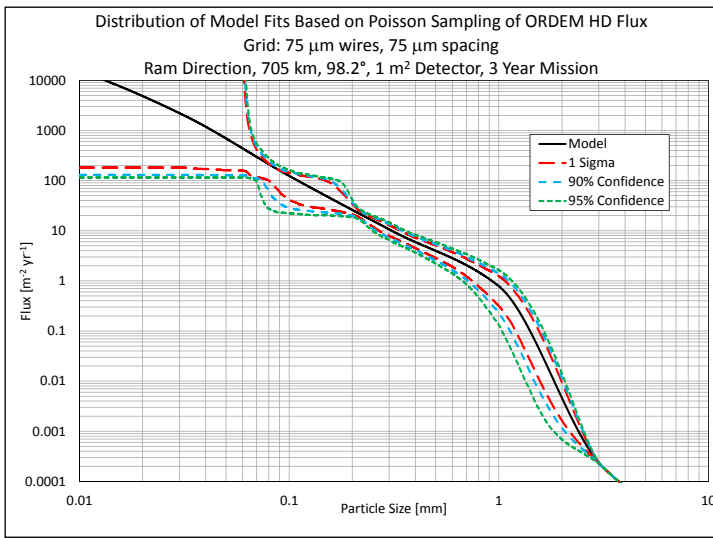


Figure 4. The estimated HD flux shows similar behavior as the MD flux in Fig. 3.

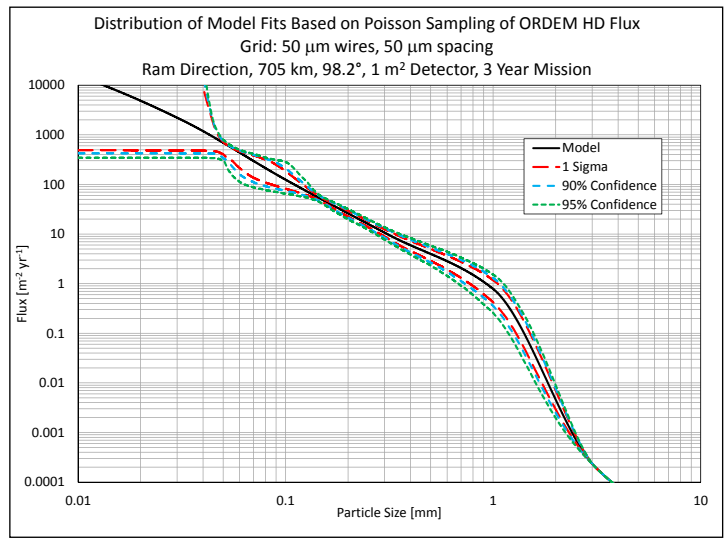


Figure 5. The estimated HD flux as in Fig. 4, but using a sensor with 50 μm wires separated by 50 μm.

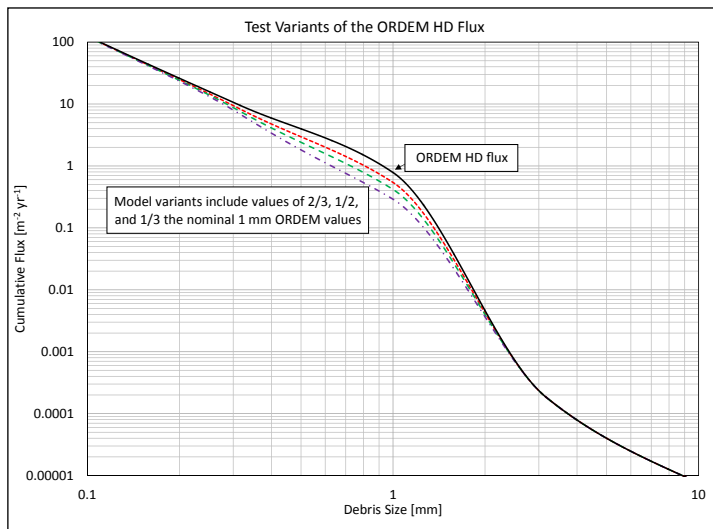


Figure 6. In an effort to study how well the instrument can resolve differences between the actual flux and ORDEM 3.0 model flux, these series of modified model fluxes are used to generate the Monte Carlo data to be compared to the model flux.

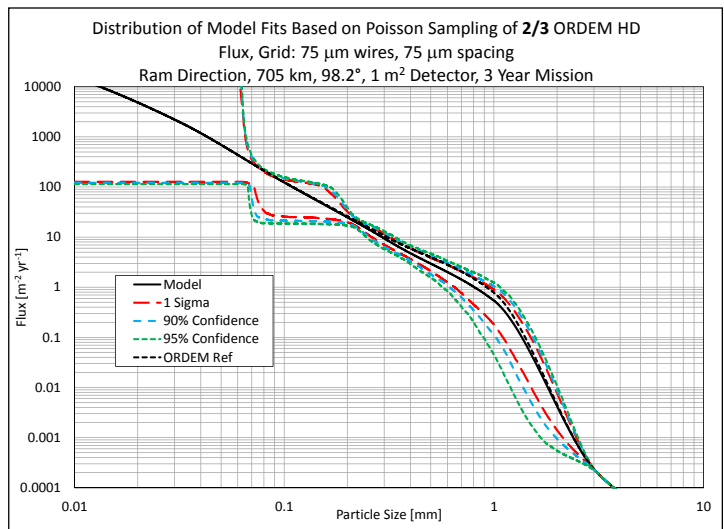


Figure 7. The dotted line shows the ORDEM flux, and the solid black line shows the modified 2/3 flux from Fig. 6. The nominal mission is incapable of resolving a flux 2/3 of the ORDEM 3.0 flux. The ORDEM reference flux is still within the 1 sigma bounds. A longer exposure in time and/or surface area would be needed to resolve this level of difference in flux.

Benefits of a High LEO

continued from page 5

flux. This can be accomplished by having more than one instrument on different spacecraft platforms to increase the total area-time product of the experiment. ♦

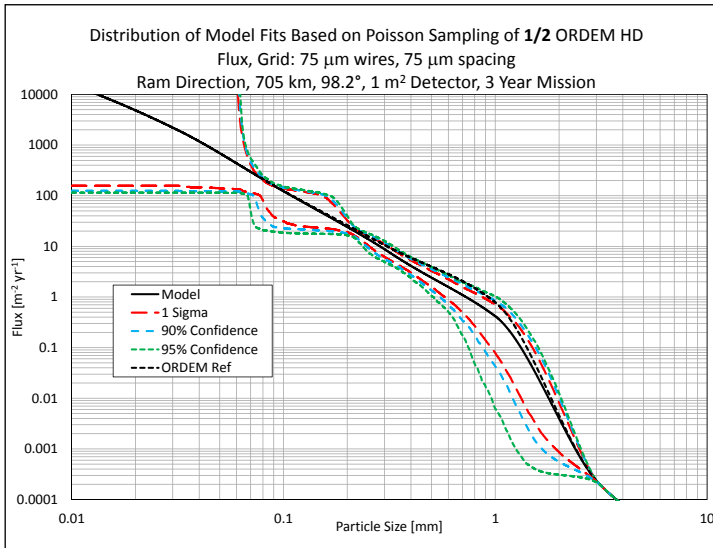


Figure 8. The dotted line shows the ORDEM flux, and the solid black line shows the modified 1/2 flux from Fig. 6. The nominal mission can partially resolve a flux 1/2 of the ORDEM 3.0 flux, at least for debris several hundred microns in size. The 1 mm flux is barely resolvable within the uncertainty bounds.

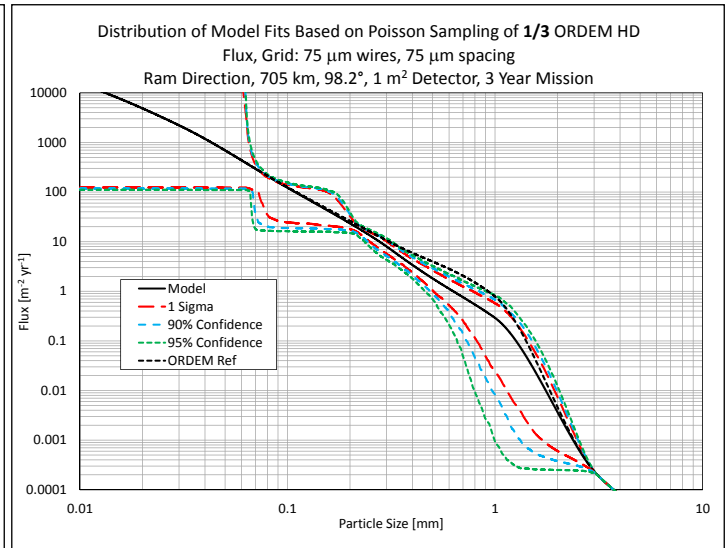


Figure 9. The dotted line shows the ORDEM flux, and the solid black line shows the modified 1/3 flux from Fig. 6. The nominal mission can resolve a flux 1/3 of the ORDEM 3.0 flux, including up to the 1 mm flux.

Debris Assessment Software (DAS) Reentry Risk Analysis: Mission Planning for Compliance with NASA Standards

J. OPIELA, C. OSTROM, AND J. MARICHALAR

This article details the NASA requirements for reentry debris casualty risk, presents a practical example, and suggests methods to mitigate this risk. NASA's framework of requirements for limiting the creation and risks of orbital debris includes limiting the risk of human casualty from reentering objects. The U.S. Government Orbital Debris Mitigation Standard Practices, Objective 4 "Postmission Disposal of Space Structures," Section 4-1 states: *If a space structure is to be disposed of by reentry into the Earth's atmosphere, the risk of human casualty will be less than 1 in 10,000* [1]. Section 1.1.3.c of the NASA Procedural Requirements for Limiting Orbital Debris, NPR 8715.6B, contains the general statement, *The risk of human casualty due to reentry of orbital debris is limited to accepted levels* [2]. The specific requirements are detailed in the NASA Technical Standard, Process for limiting Orbital Debris, section 4.7, "Survival of Debris from the Postmission Disposal Earth Atmospheric Reentry Option" [3]. Section 4.7.2 of the Standard states:

NASA space programs and projects that use atmospheric reentry as a means of disposal for space structures need to limit the amount of debris that can survive reentry and pose a threat to people on the surface of the Earth. This area applies to full spacecraft as well as jettisoned components.

4.7.2.1 *Requirement 4.7-1. Limit the risk of human casualty:* The potential for human casualty is assumed for any object with an impacting kinetic energy in excess of 15 joules:

- For uncontrolled reentry, the risk of human casualty from surviving debris shall not exceed 0.0001 (1:10,000).
- For controlled reentry, the selected trajectory shall ensure that no surviving debris impact with a kinetic energy greater than 15 joules is closer than 370 km from foreign landmasses, or is within 50 km from the continental U.S., territories of the U.S., and the permanent ice pack of Antarctica.

c. For controlled reentries, the product of the probability of failure of the reentry burn (from Requirement 4.6-4.b) and the risk of human casualty assuming uncontrolled reentry shall not exceed 0.0001 (1:10,000).

Section 4.7.3 of the Standard continues, detailing the rationale for the 15 joule limit (a value determined by the Departments of Defense and Energy, among others, to be the limit above which any strike on a person will require prompt medical attention). The uncontrolled human casualty risk limit of 1:10,000 is also currently in use by the European Space Agency and IADC, and was derived from "a comparison of U.S. Government-accepted casualty risks in other transportation and non-transportation activities." The Standard does not account for sheltering, as it is estimated that as much as 80% of the world's population is either unprotected or in lightly-sheltered structures that can protect against falling objects with low kilojoule-level kinetic energies.

continued on page 7

DAS Reentry Risk Analysis

continued from page 7

“Aluminum (generic)” and the shape is “Box”. The satellite’s mass is copied from the Mission Editor, and the user must enter the shape dimensions. Note that dimensions must be sorted by magnitude such that Length > (Diameter or Width) > Height. For the 12U satellite the length is 0.3 m, width is 0.2 m, and height is 0.2 m.

Now the user begins entering sub-items. A battery box consists of the box and its internal cells. The user selects Humphrey in the upper input area labeled “Input”, then clicks the button “Add Sub-Item” just below this input area. A new row appears in the “Component Data” input area, where the user again clicks on each cell to enable input/typing in that cell. The name of the new sub-item is “Battery Box”, quantity is 1, the material (from pull-down list) is “Aluminum (generic)”, and the shape is “Box”. This sub-component’s thermal mass is 0.5 kg. Thermal mass of a component is the

mass of the object’s outer structure only, without any internal sub-components. In the case of the battery box, this is the mass of the aluminum shell without the cells. (Note that the satellite’s total mass is its aerodynamic mass, which includes the mass of all sub-components.) The length is 0.12 m, width is 0.09 m, and height is 0.06 m.

Next the user enters the battery cells by selecting the item “Battery Box” in the Input area and clicking Add Sub-Item, creating a new row in the Component Data area. The new sub-item’s name is “Battery” and quantity is 15. The cells are modeled as cylinders of material “Stainless Steel (generic)”, with mass of 0.048 kg, length of 0.065 m, and diameter of 0.0186 m. In the list of components in the Input area, the battery now appears as a branched “child” of the battery box.

The main instrument of the satellite is a simple telescope, modeled as an aluminum tube and two

glass plates. As with the battery box, the user selects the satellite (“Humphrey”) in the upper input area and clicks Add Sub-Item. In the Component Data area, the user clicks the data cells and enters the component name “Telescope”, quantity of 2, selects material “Aluminum 7075-T6”, and object shape Cylinder. The component’s thermal mass is 1.0 kg, length is 0.15 m, and diameter is 0.08 m. Returning to the upper component list, the user selects Telescope and clicks Add Sub-Item. The new sub-component name is “Lens” and quantity is 2. At this point the user finds that the default list of materials does not include optical glass.

The user must now enter new information for a user-defined material. The user brings up the materials database either by clicking on the icon (spark on a blue cylinder) or selecting the menu item Edit → Material Database. The upper part of the Material Database window (Fig. 3) contains the names and densities (for reference) of the default DAS materials. In the lower window pane labeled “User-Defined Material”, the user clicks in a data cell before entering that cell’s data. For an ultra-low expansion glass, the user enters the name “ULE Glass”, density of 2210 kg/m³, specific heat of 776 J/kg-K, heat of fusion of 250,000 J/kg, and melting temperature of 1760 K. The user finishes the material input by clicking the Save and then Close buttons. The user-specified materials are saved with the current DAS project.

Returning to the reentry risk Component Data entry area, the user clicks twice in the Material Type cell for the Lens component and scrolls through the list to find the new material “ULE Glass”. For the object shape, the “Flat Plate” selection best fits DAS’s aerothermal model. The thermal mass is 0.11 kg, and both length and width are 0.08 m.

This process is repeated to add additional components to the satellite, including all major components such as a radiator, motherboard, solar panels, reaction wheels/gyroscopes, tanks, and piping. Small, easily destroyed items like wiring may be excluded (though their mass is included in the satellite’s total mass). Fasteners not expected to separate due to aerodynamic forces would also not be included as separate components, but their masses are included with the mass of the objects retaining the fasteners during reentry. When the satellite is selected in the upper input list, DAS indicates the fraction of the total mass that has been defined by the subcomponents.

After all the major components have been

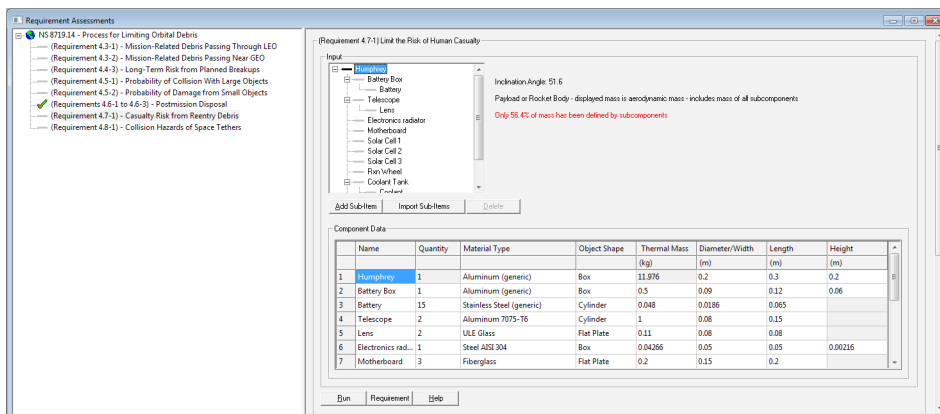


Figure 2. DAS Requirement Assessments Window.

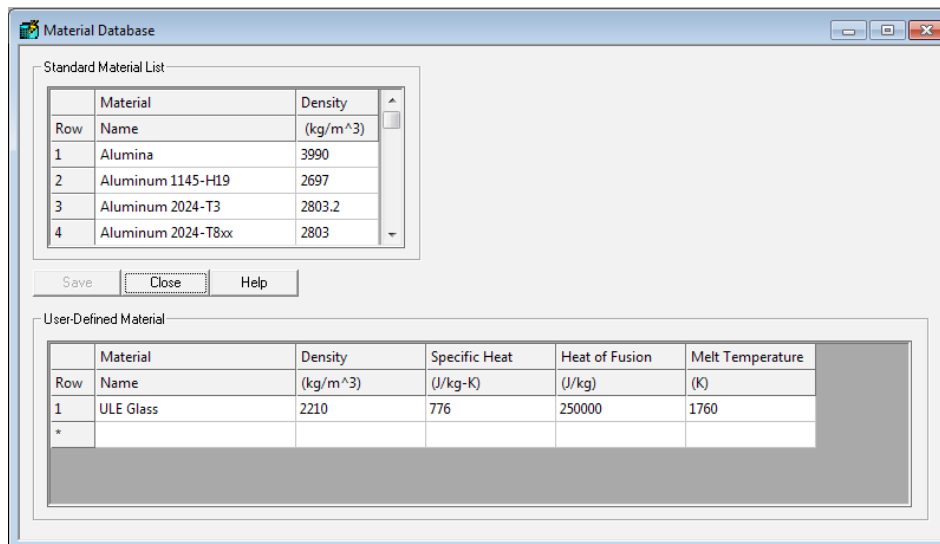


Figure 3. DAS Material Database Window.

continued on page 9

DAS Reentry Risk Analysis

continued from page 8

defined, the user will save the project and then click the Run button below the Component Data area. The model runs fairly quickly, the exact length depending on the number of components. The output pane appears below the Component Data area (see bottom of Fig. 4). Output includes the compliance status and overall risk of human casualty for each launched object (from the Mission Editor). Further, it lists the subcomponents with their demise altitudes, casualty areas, and impact kinetic energies (for objects with demise altitude of zero). Only objects that reach the ground (*i.e.*, demise altitude of zero) with kinetic energy of 15 J or greater contribute to the DCA. Of the four specific components listed above, only the glass lenses survive reentry. They impact with 31 J energy, so they contribute to the total DCA. Adding a circuit board, three solar panels, four reaction wheels, coolant and cold gas propellant tanks, and piping yields a total DCA of 2.73 m².

DAS uses the total DCA and the predicted population distribution under the satellite's orbit in the year of reentry to compute the risk of human casualty. For this example satellite, reentering in the year 2041, the risk is assessed to be 1:19,000. This result, less than the threshold of 1:10,000, is compliant with the NASA Standard. If the mission were non-compliant, or if the designer wanted to reduce impact energies, the list of components and energies would serve as a guide for design changes.

Spacecraft commonly feature arrays of battery cells, which are usually held in some kind of container. These battery boxes are typically designed to hold the batteries in place during ascent and any orbital maneuvers, but demise during reentry, releasing the battery cells to continue their

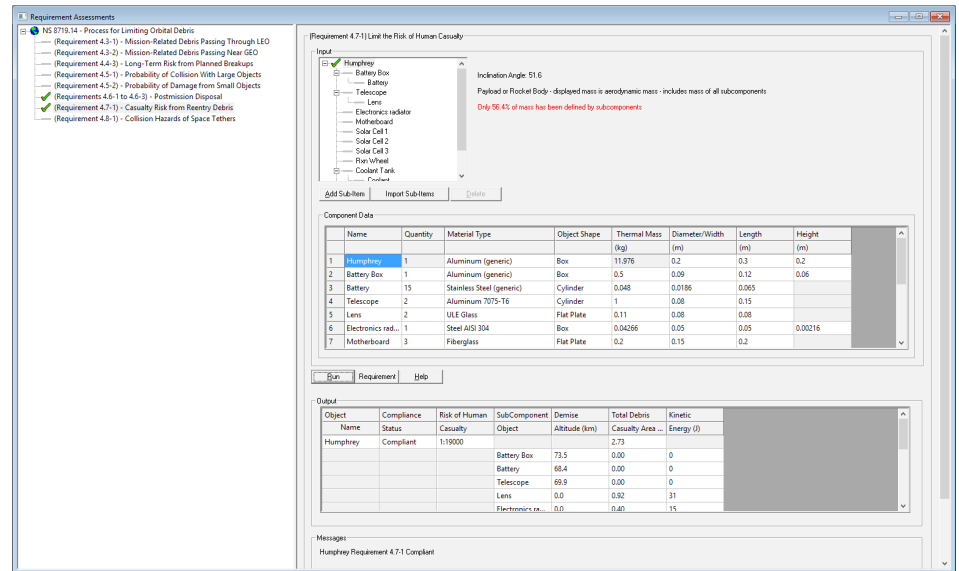


Figure 4. DAS Requirement Assessments Window, Focused on Reentry Debris Casualty Risk Results.

descent individually. However, the size, shape, and mass of these individual cells (especially the 18650 form factor which is currently popular), may result in many surviving components with lethal impact kinetic energy, like a hail of bullets. Instead, designers may consider increasing the strength or changing the material the battery boxes are made from, allowing the box to survive as a single object with the batteries inside. Though the total mass that survives from the spacecraft to impact the ground may be greater, the total DCA may be reduced, which decreases the overall casualty risk.

References

1. U.S. Government Orbital Debris

Mitigation Standard Practices (February 2001). Available at <https://www.orbitaldebris.jsc.nasa.gov/reference-documents.html>.

2. NASA Procedural Requirements for Limiting Orbital Debris and Evaluating the Meteoroid and Orbital Debris Environments, NPR 8715.6B (February 2017). Available at <https://www.orbitaldebris.jsc.nasa.gov/reference-documents.html>.

3. NASA Technical Standard Process for Limiting Orbital Debris, NASA-STD-8719.14A with Change 1 (December 2011). Available at <https://www.orbitaldebris.jsc.nasa.gov/reference-documents.html>. ♦

CONFERENCE REPORTS

The 7th European Conference on Space Debris, 18-21 April 2017, ESA/ESOC, Darmstadt, Germany

The 7th European Conference on Space Debris was held 18-21 April 2017 in Darmstadt, Germany. This meeting report includes highlights of the conference, with special emphasis on presented papers representing the NASA Orbital Debris Program Office (ODPO). Visit <https://conference.sdo.esoc.esa.int/page/programme> to see the full program.

The Opening Ceremony highlighted talks from Professor Jan Worner (European Space Agency (ESA) Director General); Dr. Rolf

Densing (Head of the European Space Operations Center (ESOC) and ESA Director of Operations); Dr. Holger Krag (Head of ESA Space Debris Office), who also presented the Space Debris Movie Premiere; and last, the keynote speaker Mr. Donald Kessler (NASA retiree).

Following the opening, representatives from various institutions and government agencies gave overviews of current research or projects in their respective organizations. The opening talk was provided by Dr. Hugh Lewis (University

of Southampton) on *Sensitivity of the Space Debris Environment to Large Constellations and Small Satellites*. Dr. J.-C. Liou [NASA Orbital Debris Program Office (ODPO)] presented *Highlights of Recent Research Activities at the NASA Orbital Debris Program Office*. The third highlighted talk was given by Dr. Satomi Kawamoto [Japan Aerospace Exploration Agency (JAXA)] on the *Current Status of Research and Development on Active Debris*

continued on page 10

7th European Conference on Space Debris

continued from page 9

Removal at JAXA. The last talk was delivered by Dr. Thomas Schildknecht (Astronomical Institute from the University of Bern) for *Determining and Modeling Space Debris Attitude State by Fusing Data from Different Observation Techniques.*

Two papers representing the NASA ODPO were presented in the Radar, Optical, and *In-situ* Measurements – Ground-based Experiments Session: Dr. Pat Seitzer (University of Michigan) presented *The Small Size Debris Population at GEO from Optical Observations* and Dr. Brent Buckalew (Jacobs JETS contract/NASA ODPO) delivered results from the *United Kingdom Infrared Telescope's Spectrograph Observations of Human-Made Space Objects.* The following day in the Radar, Optical, and *in-situ* Measurements – *In-situ* Session Mr. Joe Hamilton (NASA ODPO) presented *Development of the Space Debris Sensor (SDS).* In the Radar, Optical and *In-situ* Measurements Poster Session Dr. James Frith (University of Texas at El Paso – Jacobs JETS/NASA ODPO) presented *Observing Strategies for Focused Orbital Debris surveys*

using the Magellan Telescope and Dr. Sue Lederer (NASA ODPO) presented *Ground-based Observing Campaigns of Briz-M Debris with the UKIRT and NASA MCAT Telescopes.*

In the Hypervelocity Impacts & Shielding: Application Session Mr. Jim Hyde (JACOBS JETS/NASA HVIT) presented *Surveys of ISS Returned Hardware for MMOD Impacts.* In the Hypervelocity Impacts & Shielding: Simulations and Tests Session Dr. Heather Cowardin (University of Texas at El Paso – Jacobs JETS/NASA ODPO) presented *Characterization of Orbital Debris via Hyper-velocity Laboratory-based Tests.*

One paper from NASA ODPO was presented in the Re-entry Risk Analysis-Application Session by Dr. Jack Bacon (NASA ODPO) on *Minimum dV for Targeted Spacecraft Disposal.*

On the final day of the 4-day conference, three papers representing NASA ODPO were presented in the Debris & Meteoroid

Environment Modeling and Prediction Session: Mr. Drew Vavrin and Dr. Alyssa Manis (Jacobs -JETS/NASA ODPO) presented *Effects of CubeSat Deployments in Low-Earth Orbit,* Dr. Mark Matney (NASA ODPO) discussed *Algorithms for the Computation of Debris Risks,* and Mr. Erick Ausay (University of Florida) provided *A Comparison of the SOCIT and DebrisSat Experiments.* Mr. William Cooke (NASA Marshall Space Flight Center) also presented in this session on *A Comparison of damaging Meteoroid and Orbital Debris Fluxes in Earth Orbit.* Dr. Mark Matney (NASA ODPO) also co-chaired the final session of the conference, Debris Mitigation: Application and Processes.

Immediately following the ESA Space Debris conference, the 35th Inter-Agency Space Debris Coordination Committee (IADC) meeting was held in the same location for three consecutive days. The next ESA Space Debris Conference will be held in 2021 with the exact dates are to be determined. ♦

The 14th Hypervelocity Impact Symposium, 24-28 April 2017, Canterbury, Kent, United Kingdom

The 14th Hypervelocity Impact Symposium (HVIS) was held at the University of Kent in Canterbury, United Kingdom, on 24-28 April 2017. This year's symposium was hosted by the School of Physical Sciences at the University of Kent and attracted more than 126 attendees from government, industry, and academic organizations.

The Hypervelocity Impact Symposium consisted of 11 topical oral and poster sessions. They covered high-velocity launchers and

diagnostics; spacecraft meteoroid/debris shielding and failure analyses; material response to hypervelocity impacts; fracture and fragmentation; high-velocity penetration mechanics; armor/anti-armor and ballistic technology; and non-linear analytical/numerical methodologies for structural dynamics. A special set of three sessions was devoted to asteroid impact and planetary defense technology.

A total of 54 oral and 33 poster papers

were presented representing the community's latest efforts to better characterize hypervelocity impact phenomenology and solar system impacts. Papers specific to impact observations of returned surfaces and impact observations of operational assets were given; along with papers describing the structural response of space borne assets. The society adjourned its meeting and will reconvene in April 2019 on the Gulf coast of Alabama. ♦

The 31st International Symposium on Space Technology and Science, 5-9 June 2017, Matsuyama, Japan

The 31st International Symposium on Space Technology and Science (ISTS) took place in Matsuyama, Japan, on 5-9 June 2017. This year's ISTS was a joint conference with the 26th International Symposium on Space Flight Dynamics (ISSFD) and the 8th Nano-Satellite Symposium (NSAT), with a conference theme of "Open Up a New Age of Space Discovery." JAXA's astronaut, Mr. Takuya Ohnishi, provided a very well received keynote speech on "ISS Expedition 48/49 Mission Report and the Future of Human Spaceflight" at the Opening Ceremony.

The committee organizing the ISTS "Space Environment and Debris" sessions was chaired by Dr. Toshifumi Yanagisawa of JAXA. A total of 30 papers were presented during the space debris sessions. Those papers focused on optical observations of the debris populations, in-situ measurement modeling, long-term environment and reentry studies, hypervelocity impact tests, and active debris removal. This year's ISTS also included a special session on the 9th Global Trajectory Optimization Competition (GTOC 9). The theme of the GTOC 9 was "The Kessler

Run." More than 30 teams from around the world participated in GTOC9 to design mission scenarios to optimize the efficiency and cost for the removal of 123 pre-selected targets in sun-sync orbits. Several teams provided presentations to outline their approaches to solve the problem and their best solutions. The winner of the competition was a team from the NASA Jet Propulsion Lab (JPL)'s Outer Planets Mission Analysis group. As a tradition, the JPL team will be responsible for defining a competition topic and organizing GTOC X. ♦

UPCOMING MEETINGS

20-24 August 2017: AAS/AIAA Astrodynamics Specialist Conference, Stevenson, WA (USA)

The American Astronautical Society (AAS) and the American Institute of Aeronautics and Astronautics (AIAA) will co-host the 2017 AAS/AIAA Astrodynamics Specialist Conference in Stevenson, Washington, USA. Technical sessions include,

but are not limited to, orbit determination and space surveillance tracking; orbital debris and the space environment; orbital dynamics, perturbations, and stability; proximity operations; space situational awareness, conjunction analysis, and collision avoidance;

and satellite constellations. The abstract submission deadline passed on 24 April 2017. Additional information about the conference is available at http://www.space-flight.org/docs/2017_summer/2017_summer.html.

12-14 September 2017: AIAA Space 2017, Orlando, FL (USA)

The American Institute of Aeronautics and Astronautics (AIAA) will convene the AIAA SPACE and Astronautics Forum and Exposition (AIAA SPACE 2017) in Orlando,

Florida, USA. Technical sessions include Space Law and Policy and Space Operations. The abstract submission deadline passed on 23 February 2017. Additional information

about the conference is available at <http://space.aiaa.org/>.

19-22 September 2017: 18th Advanced Maui Optical and Space Surveillance Technologies Conference, Maui, Hawaii (USA)

The technical program of the 18th Advanced Maui Optical and Space Surveillance Technologies Conference (AMOS) will focus on subjects that are mission critical to Space Situational Awareness. The technical sessions

include papers and posters on Orbital Debris, Space Situational Awareness, Adaptive Optics & Imaging, Astrodynamics, Non-resolved Object Characterization, and related topics. The abstract submission deadline passed on

1 April 2017. Additional information about the conference is available at <http://www.amostech.com>.

25-29 September 2017: 68th International Astronautical Congress (IAC), Adelaide, Australia

The IAC will return to Australia in 2017, with a theme of "Unlocking imagination, fostering innovation and strengthening security." The IAA will again organize the Symposium On Space Debris during the congress. Nine sessions are planned to cover

all aspects of orbital debris activities, including measurements, modeling, hypervelocity impact, mitigation, remediation, and policy/legal/economic challenges for environment management. An additional joint session with the Symposium on Small Satellite Missions is

under consideration. The abstract submission deadline passed on 28 February 2017. Additional information for the 2017 IAC is available at: <http://www.iac2017.org/>.

18-20 October 2017: 9th International Association for the Advancement of Space Safety (IAASS) Conference, Toulouse, France

The 9th conference of the IAASS has as its theme "Know Safety, No Pain". Major debris-related topics include designing safety into space vehicles, space debris remediation, re-entry safety, nuclear safety for space missions, safety risk management and probabilistic risk

assessment, and launch and in-orbit collision risk. In addition to the main sessions, four specialized sections will address Space Debris Reentries, Space Traffic Management, Safety Standards for Commercial Human Spaceflight, and Human Performance and Safety. The

abstract submission deadline passed on 30 May 2017. Additional information for the 2017 IAC is available at: <http://iaassconference2017.space-safety.org/>.

13-15 November 2017: 1st IAA Conference on Space Situational Awareness (ICSSA), Orlando, FL (USA)

The International Academy of Astronautics (IAA) and the American Institute of Aeronautics and Astronautics (AIAA) will convene the 1st IAA Conference on Space Situational Awareness in Orlando, Florida, USA. Co-sponsors include the University of

Florida, the University of Arizona, the Ohio State University, the University of Central Florida, and Texas A&M University. Technical sessions include, but are not limited to, resident space object sensing, identification, forecasting, tracking, risk assessment, debris removal, drag

assisted reentry, and deorbiting technologies. The abstract submission deadline passed on 30 June 2017. Additional information about the conference is available at <http://www.aiaa.org/icssa2017/> and <http://reg.conferences.dce.ufl.edu/ICSSA/1357>.

SATELLITE BOX SCORE

(as of 4 April 2017, cataloged by the
U.S. SPACE SURVEILLANCE NETWORK)

Country/ Organization	Payloads	Rocket Bodies & Debris	Total
CHINA	250	3594	3844
CIS	1509	4997	6506
ESA	75	58	133
FRANCE	63	482	545
INDIA	82	115	197
JAPAN	162	96	258
USA	1529	4689	6218
OTHER	825	114	939
TOTAL	4495	14145	18640

DAS 2.1 NOTICE

Attention DAS 2.1 Users: an updated solar flux table is available for use with DAS 2.1. Please go to the Orbital Debris Website at <https://orbitaldebris.jsc.nasa.gov/mitigation/das.html> to download the updated table and subscribe for email alerts of future updates.

Technical Editor
Phillip Anz-Meador, Ph.D.

Managing Editor
Debi Shoots



**Correspondence concerning
the ODN can be sent to:**

NASA Johnson Space Center
The Orbital Debris Program Office
Attn: Debi Shoots, MC XI4-B9E
Houston, TX 77058



debra.d.shoots@nasa.gov



National Aeronautics and Space Administration
Lyndon B. Johnson Space Center
2101 NASA Parkway
Houston, TX 77058

www.nasa.gov
<http://orbitaldebris.jsc.nasa.gov/>

INTERNATIONAL SPACE MISSIONS

1 April 2017 – 30 June 2017

International Designator	Payloads	Country/ Organization	Perigee Altitude (KM)	Apogee Altitude (KM)	Inclination (DEG)	Earth Orbital Rocket Bodies	Other Cataloged Debris
2017-018A	CHINASAT 16	CHINA	35768	35805	0.1	1	0
2017-019A	CYGNUS OA-7	USA	387	403	51.6	0	0
2017-019B	OBJECT B*	USA	476	491	51.6		
2017-019C	OBJECT C*	USA	476	491	51.6		
2017-019D	OBJECT D*	USA	476	492	51.6		
2017-019E	OBJECT E*	USA	476	491	51.6		
2017-020A	SOYUZ MS-04	RUSSIA	401	408	51.6	1	0
2017-021A	TIANZHOU 1	CHINA	392	395	42.8	1	3
2017-022A	USA 276	USA	NO ELEMS. AVAILABLE			1	0
2017-023A	KOREASAT 7	SOUTH KOREA	35787	35788	0.0	1	1
2017-023B	SGDC	BRAZIL	35785	35791	0.0		
2017-024A	GSAT 9	INDIA	35774	35799	0.1	1	0
2017-025A	INMARSAT 5-F4	INMARSAT	31280	40340	0.2	1	0
1998-067LH 1998-067LJ-LZ	SOMP2 (16 additional CubeSats deployed from 1)	GERMANY VARIOUS	394	404	51.6	0	0
2017-026A	SES 15	SES	EN ROUTE TO GEO			1	0
2017-027A	COSMOS 2518	RUSSIA	1686	38667	63.8	1	0
1998-067MA 1998-067MB-MS	CHALLENGER (16 additional CubeSats deployed from 1)	USA VARIOUS	394	405	51.6	0	0
2017-028A	QZS-2	JAPAN	32620	38963	44.7	1	0
2017-029A	VIASAT 2	USA	16871	54455	0.4	1	1
2017-029B	EUTELSAT 172B	EUTELSAT	2192	38761	4.8		
2017-030A	DRAGON CRS-11	USA	392	407	51.6	0	2
2017-031A	GSAT 19	INDIA	35773	35801	0.0	1	0
2017-032A	ECHOSTAR 21	USA	35779	35793	7.5	1	1
2017-033A	PROGRESS MS-06	RUSSIA	401	408	51.6	1	0
2017-034A	HXMT	CHINA	538	547	43.0	1	0
2017-034B	ZHUHAI-1 02	CHINA	535	544	43.0		
2017-034C	NUSAT-3	ARGENTINA	536	544	43.0		
2017-034D	ZHUHAI-1 01	CHINA	535	544	43.0		
2017-035A	CHINASAT 9A	CHINA	EN ROUTE TO GEO			1	0
2017-036A-AH	(CARTOSAT 2E & small secondary payloads)	INDIA & Various	503	521	97.5	0	0
2017-037A	COSMOS 2519	RUSSIA	653	670	98.1	2	0
2017-038A	BULGARIASAT-1	BULGARIA	35709	35951	0.1	1	0
2017-039A	IRIDIUM 113	USA	607	625	86.7	0	0
2017-039B	IRIDIUM 123	USA	607	625	86.7		
2017-039C	IRIDIUM 120	USA	608	625	86.7		
2017-039D	IRIDIUM 115	USA	606	626	86.7		
2017-039E	IRIDIUM 118	USA	609	625	86.7		
2017-039F	IRIDIUM 117	USA	606	625	86.7		
2017-039G	IRIDIUM 126	USA	606	625	86.7		
2017-039H	IRIDIUM 124	USA	608	626	86.7		
2017-039J	IRIDIUM 128	USA	609	625	86.7		
2017-039K	IRIDIUM 121	USA	609	625	86.7		
2017-040A	HELLAS-SAT 3	ESA	35557	35764	0.0	1	1
2017-040B	GSAT 17	INDIA	35464	35849	0.1		

* Identification of these objects has not been resolved